

## **Electrochemical Behaviour of Ti-20Nb-10Zr-5Ta Alloy in Simulated Physiological Fluids after Anodic Electrolytic Oxidation**

*Monica Popa, Cora Vasilescu, Silviu Iulian Drob<sup>\*</sup>, Jose M. Calderon Moreno*

Institute of Physical Chemistry "Ilie Murgulescu" of Romanian Academy, Spl. Independentei 202, PO BOX 12-194, 060021 Bucharest, Romania

\*E-mail: [sidrob@chimfiz.icf.ro](mailto:sidrob@chimfiz.icf.ro)

*Received:* 6 February 2013 / *Accepted:* 12 March 2013 / *Published:* 1 April 2013

---

In this paper, the anodic galvanostatic electrolytic method was applied on the new Ti-20Nb-10Zr-5Ta alloy (containing only non-toxic and non-allergic elements) surface; microstructure (by XRD) and morphology (by SEM) of the obtained layer was analysed. Also, the electrochemical behaviour (by potentiodynamic and linear polarisation and electrochemical impedance spectroscopy) of the galvanostatic oxidation Ti-20Nb-10Zr-5Ta alloy and the characterisation of the coating that grew on the alloy surface after 300 immersion hours in simulated physiological fluids are presented. All main electrochemical parameters became more favourable with the prolonged soaking time, due to the increase of the protective nature of the oxidation layer as result of the new depositions from the biofluids (by SEM). An electric equivalent circuit with two time constants was modelled: the first constant is for the electrodeposited barrier layer and the second constant characterises the porous layer deposited from solution. SEM micrographs and EDS elemental analysis showed that the coating formed after 300 immersion hours in Ringer and Ringer-Brown solutions contained calcium phosphates, precursors of the hydroxyapatite, the main inorganic component of the human bone, namely, the alloy surface became bioactive.

---

**Keywords:** film morphology and composition, EIS, Ringer and Ringer-Brown solutions.

### **1. INTRODUCTION**

Over the past 20 years, titanium and its Ti-6Al-4V, Ti-6Al-7Nb, Ti-13Nb-13Zr alloys have been used as implant materials due to their excellent corrosion resistance in the human biofluid and good biocompatibility. But, many cases of implant failures were registered because of the lack of the initial bonding between the implant surface and the living bone. Thus, a surface processing to improve

bone bonding ability of the implant was necessary. Different treatments were studied among these, coatings applied by plasma spray, surface implantation, chemical deposition, heat treatment, etc.; the problem of these methods are the formation of cracks and a low adhesion of these coatings with the metallic substrate. Recently, the electrolytic methods which induce the formation of the very adherent titanium dioxide,  $\text{TiO}_2$  were developed; a roughed surface with pores, which can assure the bone cell proliferation results. This dioxide can be obtained by anodic potentiostatic and galvanostatic oxidation.

Anodic potentiostatic oxidation [1-6] was performed especially in phosphoric acid solutions and optimising the electrodeposition conditions, the subsequent deposition of apatite from simulated body fluid was observed. Anodic galvanostatic oxidation [7-9] has the capacity to form a porous surface by the controlling of the current density, voltage and solution temperature, pH, content (phosphoric acid or different phosphates). By these electrolytic methods, the ions from solutions can be incorporated into the electrodeposited layer, enhancing both protective properties and bioactivity of this layer. However, the substrate content and mechanical properties has an important part for the long-term success of an implant; the alloy must contain only non-toxic and non-allergic elements Ti, Ta, Nb, Zr, Pd, Au [10, 11], to have the density and Young's modulus very closed with those of the bone and proper mechanical properties for durability, load bearing capacity, etc.

In this paper, the anodic galvanostatic electrolytic method was applied on the new Ti-20Nb-10Zr-5Ta (containing only non-toxic and non-allergic elements) alloy surface; microstructure (by X-ray diffraction - XRD) and morphology (by scanning electron microscopy - SEM) of the obtained layer was analysed. Also, the electrochemical behaviour (by potentiodynamic and linear polarisation and electrochemical impedance spectroscopy - EIS) of the galvanostatic oxidation Ti-20Nb-10Zr-5Ta alloy and the characterisation of the coating (by SEM and energy dispersive X-ray spectroscopy - EDS) that grew on the alloy surface after 300 immersion hours in simulated physiological fluids are presented.

## 2. EXPERIMENTAL

### 2.1. Anodic galvanostatic polarisation and oxidation layer obtaining

The new Ti-20Nb-10Zr-5Ta alloy was obtained by double vacuum melting in a semi-levitation furnace; this alloy has a low Young's modulus of 59 GPa and very good mechanical properties [12]. From the casting ingots were cut the cylindrical electrodes which were grinded with emery paper of different granulations, till 2000 and were polished with aluminium oxide till mirror surface; then, the electrodes were ultrasonically degreased in acetone and bi-distilled water for 15 min., dried in air and mounted in a Stern-Makrides mount system.

The anodic galvanostatic polarisation was applied by a high power, current source (MATRIX, China); the current densities of  $5 \text{ mA/cm}^2$  or  $10 \text{ mA/cm}^2$  were maintained for different time periods of 15, 35, 45, 60 minutes between to the working electrode, Ti-20Nb-10Zr-5Ta alloy and platinum auxiliary electrode. The anodisation solutions contained orthophosphoric acid  $\text{H}_3\text{PO}_4$  of 0.3M and 1M concentrations. Different layers were obtained controlling the solution concentration, current density and electrodeposition time and the layer with the most favourable structural and morphological

properties was selected and its electrochemical behaviour and corrosion resistance in different simulated physiological solutions was determined.

## 2.2. Microstructure and morphology of the oxidation layer

The X-Ray diffraction patterns were recorded with a Rigaku Ultima IV, Diffractometer  $\theta$ -2 $\theta$  using  $\text{CuK}\alpha$   $\lambda=1.5406 \text{ \AA}$  radiation over the range  $10 < 2\theta/\text{degrees} < 70$  at 40 kV and 30 mA.

The morphology of the oxidation layer and of the layers formed after different immersion periods in Ringer and Ringer-Brown solutions was analysed by scanning electron microscopy (SEM) using a Zeiss EVO-LF10 apparatus working at an accelerating voltage of 15 kV, equipped with a link energy dispersive X-ray system (EDS) for the elemental chemical analysis.

## 2.3. Electrochemical behaviour of the oxidation layer in simulated physiological fluids

The behaviour of the oxidation layer was studied in neutral Ringer and Ringer-Brown solutions and alkaline Ringer solution simulating the severe functional conditions of an implant. Ringer solution composition was (g/L): NaCl – 6.8; KCl – 0.4;  $\text{CaCl}_2$  – 0.2;  $\text{MgSO}_4 \cdot 7\text{H}_2\text{O}$  – 0.2048;  $\text{NaH}_2\text{PO}_4 \cdot \text{H}_2\text{O}$  – 0.1438;  $\text{NaHCO}_3$  -1.1; glucose – 1; pH =7.58; pH = 8.91 was obtained by KOH addition. Ringer-Brown solution composition was (g/L): NaCl – 6.0; KCl – 0.4;  $\text{CaCl}_2$  – 0.2; sodium lactate – 3.05; pH = 7.4.

The electrochemical behaviour of the oxidation layer was obtained from cyclic potentiodynamic polarisation curves, linear polarisation (Tafel representation) and electrochemical impedance spectroscopy (EIS).

The cyclic potentiodynamic polarisation was applied starting from -0.5 V to +4 V (vs. SCE) with a scan rate of 1 mV/sec. Voltalab 80 equipment with its VoltaMaster 4 program were used. From voltammograms, the main electrochemical parameters were determined:  $E_{\text{corr}}$  - corrosion potential, like zero current potential,  $E_p$  – passivation potential at which the current density is constant;  $|E_{\text{corr}} - E_p|$  difference represents the tendency to passivation (low values characterise a good, easy passivation);  $\Delta E_p$  – passive potential range of the constant current;  $j_p$  – passive current density.

The linear polarisation was performed for  $\pm 100$  mV around the open circuit potential at a scan rate of 1 mV/s using the same Voltalab 80 equipment. VoltaMaster 4 program directly supplies the values of the corrosion current density,  $j_{\text{corr}}$ , corrosion rate,  $V_{\text{corr}}$  and polarisation resistance,  $R_p$ . Ion release rates were calculated [13-16].

All electrochemical impedance spectroscopy measurements were carried out with the same Voltalab 80 equipment. A sine wave of 15 mV was applied to the working electrode at the open circuit potential of the system (measured versus saturated calomel electrode - SCE). The spectra were acquired in the  $10^5 \text{ Hz} - 10^{-1} \text{ Hz}$  frequency range. The impedance spectra were displayed as Nyquist and Bode (impedance modulus and phase angle vs. frequency) diagrams [13-16].

### 3. RESULTS AND DISCUSSIONS

#### 3.1. Microstructure and morphology of the oxidation layers

X-ray diffractograms for the oxidation layers obtained by the anodic galvanostatic polarisation at  $10 \text{ mA/cm}^2$ , for 45 min. in 0.3M and 1M  $\text{H}_3\text{PO}_4$  solutions showed no feature spectra, namely the electrodeposited film is amorphous.

SEM micrographs revealed that the oxidation layers obtained from 0.3M  $\text{H}_3\text{PO}_4$  solution (Fig. 1) is a continuous layer with a superficial porosity of submicron size and circular and homogeneous geometry; the layer obtained from 1M  $\text{H}_3\text{PO}_4$  solution (Fig. 2) has a non-uniform porosity with macropores of about  $100 \mu\text{m}$ , indicating the formation of a thick layer with a higher thickness than that in 0.3M  $\text{H}_3\text{PO}_4$  solution; the detailed micrographs demonstrate the presence of some submicron crystals that represent the anatase inclusions.

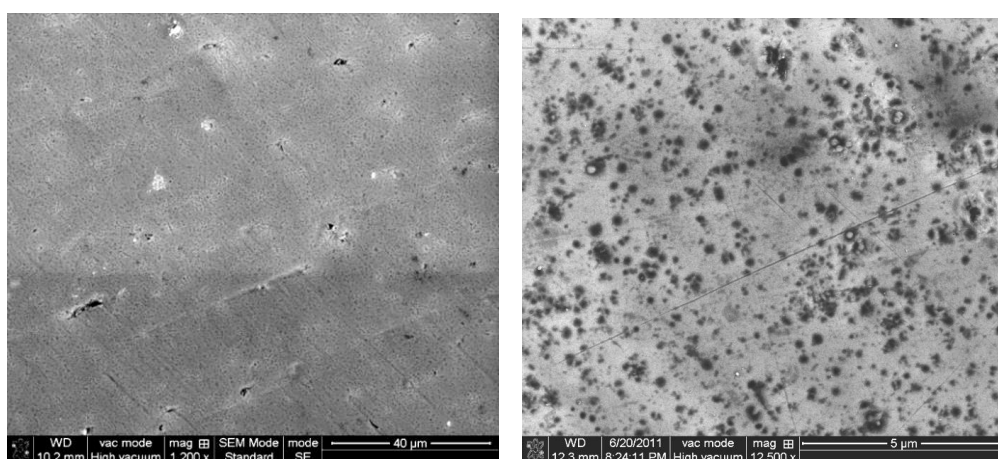


**Figure 1.** SEM micrographs for the layer electrodeposited from 0.3M  $\text{H}_3\text{PO}_4$  solution at different magnifications.

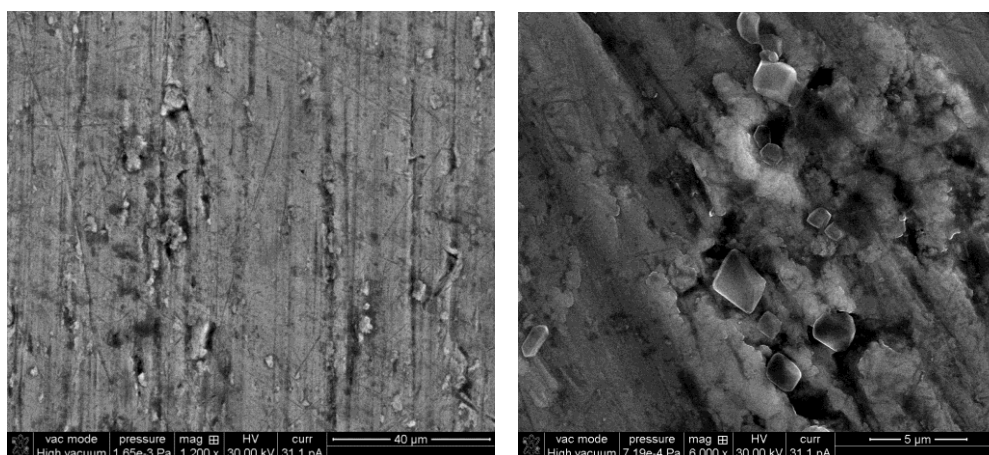


**Figure 2.** SEM micrographs for the layer electrodeposited from 1M  $\text{H}_3\text{PO}_4$  solution different magnifications.

The best oxidation layer with the most favourable microstructural and morphological properties was the layer electrodeposited from 1M H<sub>3</sub>PO<sub>4</sub> solution at 10 mA/cm<sup>2</sup>, for 45 min. Its electrochemical behaviour, corrosion resistance in different simulated physiological solutions will be reported below.

### 3.2. Electrochemical behaviour of the galvanostatic oxidation Ti-20Nb-10Zr-5Ta alloy in simulated physiological fluids

#### 3.2.1. Electrochemical behaviour of the galvanostatic oxidation Ti-20Nb-10Zr-5Ta alloy from cyclic potentiodynamic polarisation curves

Cyclic potentiodynamic polarisation curves were obtained on bare and electrolytic oxidation Ti-20Nb-10Zr-5Ta alloy after different soaking periods (24 h, 100 h and 300 h) in neutral Ringer and Ringer-Brown solutions and alkaline Ringer solution. All curves (Fig. 3) exhibited spontaneous passive behaviour with a very large passive potential range (over +4.0 V, maximum limit in our experiments) and no hysteresis, no local (pitting) corrosion [17]. Corrosion,  $E_{\text{corr}}$  and passivation,  $E_{\text{p}}$  potentials revealed more electropositive values for the galvanostatic oxidation alloy than those for the bare one (Table 1) due to the passivation action of the oxidation layer. These potentials became more electropositive for the treated alloy and slowly more electronegative for the bare alloy with the prolonged soaking time, proving the increase of the protective nature of the oxidation layer due to a new layer deposited from solutions [18-21]. Tendency to passivation,  $|E_{\text{corr}} - E_{\text{p}}|$  presented lower values for the oxidation alloy, namely an easier passivation than that of the bare alloy. Oxidation alloy had lower passive current densities,  $j_{\text{p}}$  than those of the bare alloy (Table 1), as result of the protective action of the formed oxidation layer. In time, the passivation current densities decreased, indicating that the oxidation layer thickened with new deposited layer [18-21]; for bare alloy, the variations of the passive current densities had the opposite tendencies due to some dissolution – repassivation processes [20, 21], but remained to very low values.

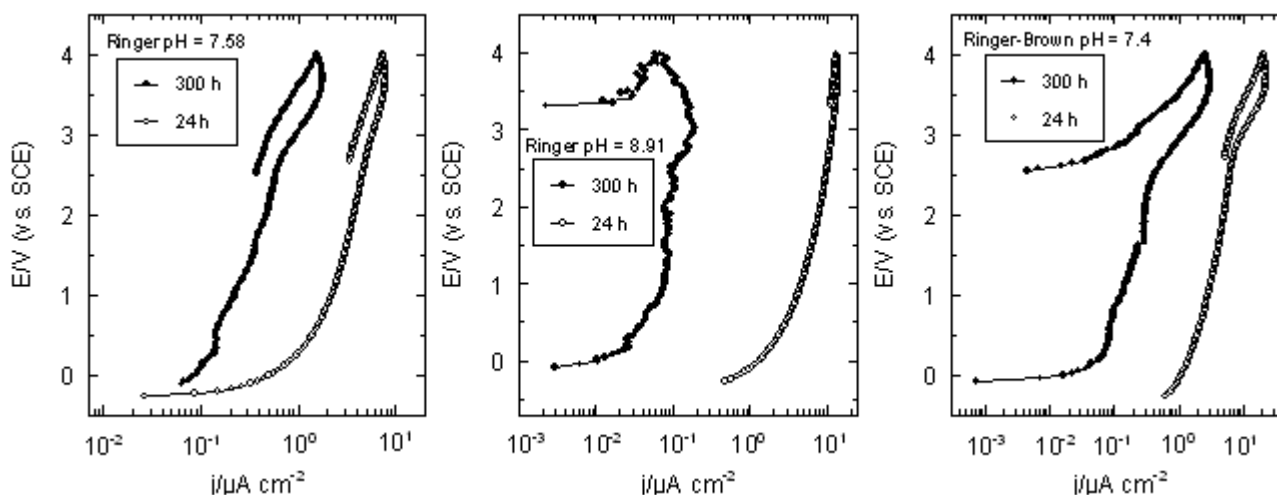


**Figure 3.** Potentiodynamic polarization curves for galvanostatic oxidation Ti-20Nb-10Zr-5Ta alloy in physiological solutions of different pH values at 37°C.

**Table 1.** Main electrochemical parameters for bare and galvanostatic oxidation Ti-20Nb-10Zr-5Ta alloy in physiological solutions of different pH values at 37°C.

Alloy	Time/h	$E_{\text{corr}}/\text{mV}$	$E_p/\text{mV}$	$ E_{\text{corr}} - E_p /\text{mV}$	$\Delta E_p/\text{mV}$	$j_p/\mu\text{A cm}^{-2}$
Ringer pH = 7.58						
Bare	24	-320	-300	20	>4000	2.20
	100	-345	-320	25	>4000	2.25
	300	-385	-360	25	>4000	2.3
Galvanostatic oxidation	24	-217	-205	12	>4000	1.80
	100	-150	-135	15	>4000	1.10
	300	-90	-80	10	>4000	0.32
Ringer pH = 8.91						
Bare	24	-340	-320	20	>4000	5.50
	100	-365	-340	25	>4000	5.55
	300	-387	-355	32	>4000	5.60
Galvanostatic oxidation	24	-227	-210	17	>4000	4.60
	100	-180	-165	15	>4000	2.50
	300	-120	-110	10	>4000	0.90
Ringer-Brown pH = 7.4						
Bare	24	-315	-300	15	>4000	2.10
	100	-340	-320	20	>4000	2.20
	300	-383	-360	23	>4000	2.25
Galvanostatic oxidation	24	-175	-160	15	>4000	1.50
	100	-110	-100	10	>4000	0.35
	300	-70	-60	10	>4000	0.15

All electrochemical parameters revealed more favourable values for the oxidation alloy than for the bare one, confirming a nobler behaviour of the treated alloy. These facts can be explained by the barrier properties of the formed oxidation layer; moreover, because all parameters exhibited more favourable values in time, it resulted that the electrodeposited layer became more densely and thickly, i.e. more resistant due to the new depositions from the solutions [22].

### 3.2.2. Corrosion resistance of the galvanostatic oxidation Ti-20Nb-10Zr-5Ta alloy from linear polarisation measurements

The corrosion  $V_{\text{corr}}$  and ion release rates [15] for the galvanostatic oxidation Ti-20Nb-10Zr-5Ta alloy had lower values than those of the bare one (Table 2) due to the enhancement of protective properties of the oxidation layer as result of its thickening by new depositions from the physiological solutions [23-25]. The values of the polarisation resistances increased and corrosion and ion release rates decreased in time, indicating the thickening of the oxidation layer.

**Table 2.** Corrosion and ion release rates for bare and galvanostatic oxidation Ti-20Nb-10Zr-5Ta alloy in physiological solutions of different pH values at 37°C.

Solution	Alloy	$j_{corr}$ $\mu\text{A}/\text{cm}^2$	$V_{corr}$ $\mu\text{m}/\text{Y}$	Resistance class	Ion release $\text{ng}/\text{cm}^2$	$R_p$ $\text{k}\Omega \text{ cm}^2$
Ringer pH = 7.58	Bare	0.089	0.783	PS	79.55	23.7
	Oxidation	0.011	0.097	PS	9.86	187.3
Ringer pH = 8.91	Bare	0.103	0.906	VS	92.05	18.6
	Oxidation	0.015	0.132	PS	13.41	168.5
Ringer-Brown pH = 7.4	Bare	0.075	0.660	PS	67.06	21.9
	Oxidation	0.0099	0.087	PS	8.84	285.3

VS – Very Stable; PS – Perfect Stable

3.2.3. Electrochemical behaviour of the galvanostatic oxidation Ti-20Nb-10Zr-5Ta alloy from the electrochemical impedance spectra

Nyquist (Fig. 4) and Bode (Fig. 5) spectra were obtained for the galvanostatic oxidation Ti-20Nb-10Zr-5Ta alloy after different immersion periods (up to 300 h) in those three physiological solutions.

Nyquist plots (Fig. 4) displayed incomplete semicircle (with some distortions) with very large diameters, typically for a capacitive behaviour, a passive protective layer. The impedance values increased with the immersion time in the simulated biofluids, revealing an increase of the layer thickness due to the new depositions from solutions; i. e., the layer became thicker and more stable [26] and acted as a protective layer between the metallic substrate and the human electrolyte, improving the substrate corrosion resistance.

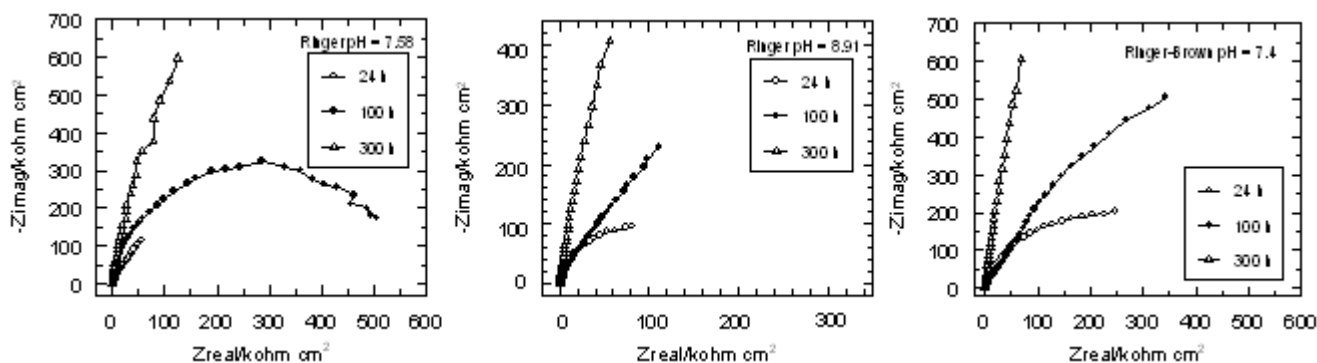
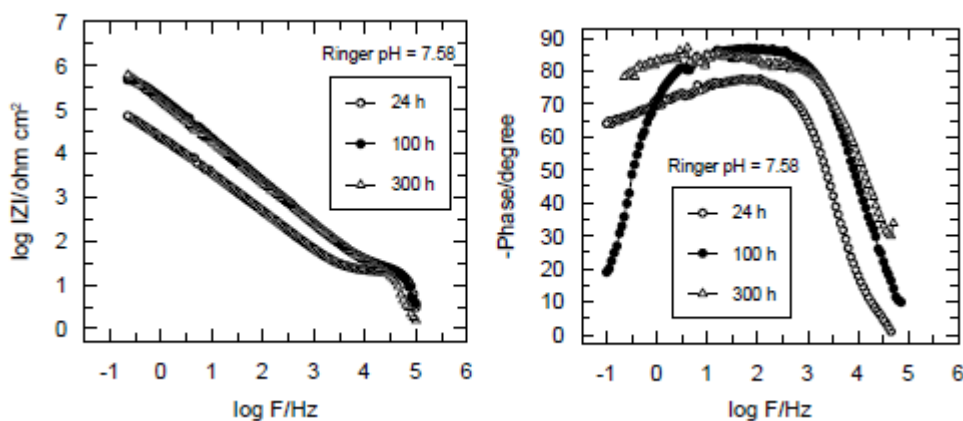


**Figure 4.** Nyquist spectra for galvanostatic oxidation Ti-20Nb-10Zr-5Ta alloy in physiological solutions of different pH values at 37°C.

Concerning Bode spectra, it is known [23] that in the low and middle frequency region (0.01-10 Hz), a phase angle of almost  $-90^0$  and a slope  $\approx -1$  show a capacitive response, i. e. a barrier passive layer. In the middle frequency region (10-100 KHz), a distinct phase angle indicates a porous layer

[18, 27]. Bode phase angle plots (Fig. 5) in the low frequency range exhibited phase angles from  $-86^{\circ}$  to  $-78^{\circ}$  in Ringer solution of pH = 7.58, from  $-85^{\circ}$  to  $-73^{\circ}$  in Ringer solution of pH = 8.91, from  $-88^{\circ}$  to  $-74^{\circ}$  in Ringer-Brown solution of pH = 7.4, proving a highly capacitive behaviour, a very stable, protective film [28]. Phase angles in the low frequency range, increased with the soaking time as result of the improvement of the film protective properties. In the medium frequency range new phase angles were registered; their values increased in time from  $-75^{\circ}$  to  $-81^{\circ}$  in neutral Ringer solution, from  $-72^{\circ}$  to  $-80^{\circ}$  in alkaline Ringer solution and from  $-75^{\circ}$  to  $-82^{\circ}$  in neutral Ringer-Brown solution. Phase angles in the middle frequency range represent the porous layers formed by the new depositions from solutions [18, 19, 28]. Bode impedance plots evinced in the low and middle frequency range, a linear variation with a slope of about -1 due to the capacitive behaviour of the surface film. The impedance values at high frequencies gradually increased with the immersion time, which represent the formation of a stable film; we can conclude that a new protective layer is formed on the barrier layer [18, 19]. Therefore, the coating on the Ti-20Nb-10Zr-5Ta alloy surface consists from two layers: an inner barrier and an outer porous layer [18, 28, 29].

An electric equivalent circuit (Fig. 6) with two time constants [29-31] was modelled: the first constant is represented by the barrier layer resistance  $R_b$  and capacitance  $CPE_b$  and the second constant is illustrated by the porous layer resistance  $R_p$  and capacitance  $CPE_p$ . Fitting parameters (Table 3) showed that the barrier layer resistance  $R_b$  is higher than the porous layer resistance  $R_p$ , indicating that the anticorrosive resistance is provided by the barrier layer. Both barrier and porous layers resistances increased in time due to the compactness of the barrier layer and respectively to the precipitation of some compounds from solution inside the pores. Resistance of the solution  $R_{sol}$  slowly decreased in time as result of the ion deposition on the primary oxidation layer. Capacitances of the barrier  $CPE_b$  and porous  $CPE_p$  layers very slowly decreased in time, proving that the capacitive behaviour of the coating was not affected by the immersion time. The values of the frequency independent parameter  $n_b$  were much closed to 1 ( $n \approx 0.9$ ) and indicate a capacitive behaviour, a passive, protective stable film formed on the Ti-20Nb-10Zr-5Ta alloy surface; the parameter  $n_p$  had lower values than  $n_b$  and shows a porous layer [28].



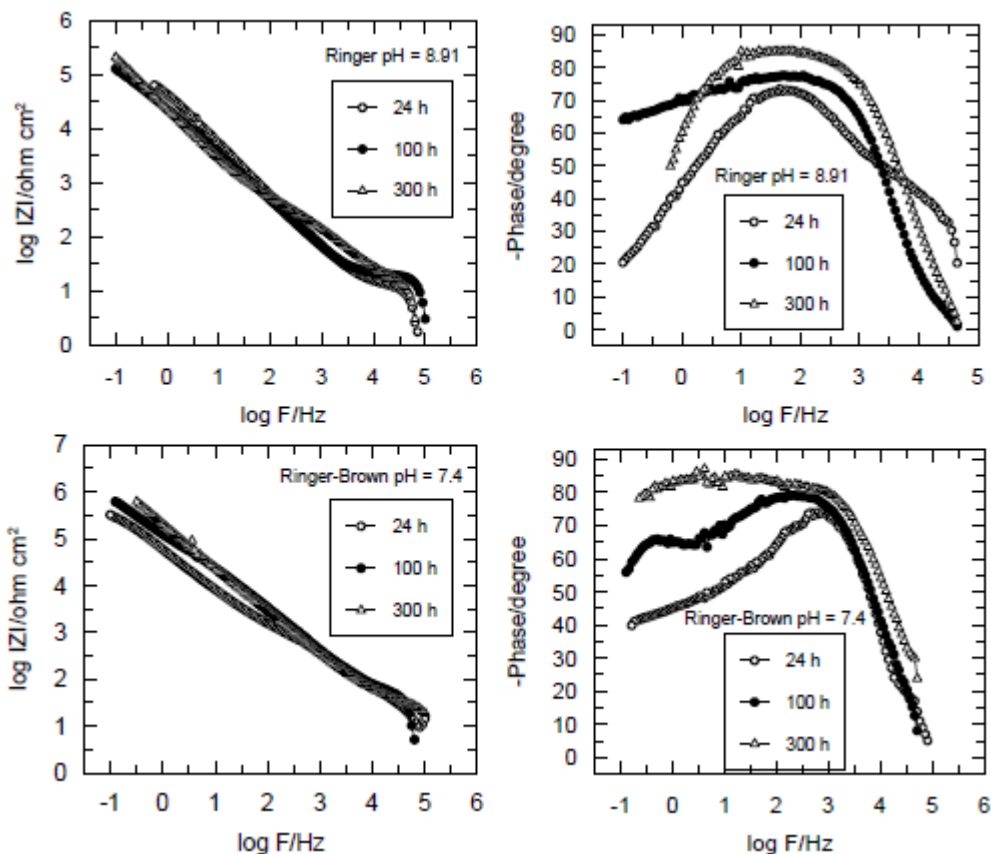


**Figure 5.** Bode spectra for galvanostatic oxidation Ti-20Nb-10Zr-5Ta alloy in physiological solutions of different pH values at 37<sup>0</sup>C.

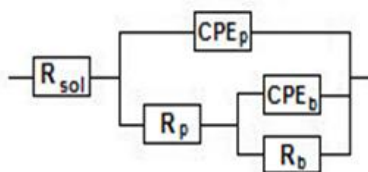


**Figure 6.** Electric equivalent circuit

*3.3. Morphology and composition of the coating deposited on the galvanostatic oxidation Ti-20Nb-10Zr-5Ta alloy surface after immersion in simulated physiological fluids*

SEM micrographs of the galvanostatic oxidation Ti-20Nb-10Zr-5Ta alloy surface after immersion in neutral Ringer solution for 300 h (Fig. 7) showed the deposition of a continuous coating with some protruding rounded features; EDS elemental analysis detected the presence of Ca, P and O as the main coating elements, as well as smaller contents of Na, Mg and Si. The composition of the observed rounded features is the same than the rest of the coating. Samples immersed for 300 h in Ringer solution of basic pH (pH = 8.91), and in neutral Ringer-Brown solution, revealed similar microstructural features (Fig. 8) and elemental composition.

**Table 3.** Fitting parameters for the two time constants electric equivalent circuit.

Time/h	$R_{sol}/\Omega\text{ cm}^2$	$R_b/\Omega\text{ cm}^2$	$CPE_b/S\text{ s cm}^{-2}$	$n_b$	$R_p/\Omega\text{ cm}^2$	$CPE_p/S\text{ s cm}^{-2}$	$n_p$
<b>Ringer pH = 7.58</b>							
24	17.8	$3.5 \times 10^6$	$4.1 \times 10^{-5}$	0.91	190.8	$6.2 \times 10^{-5}$	0.83
100	17.4	$8.9 \times 10^6$	$3.2 \times 10^{-5}$	0.93	483.6	$4.5 \times 10^{-5}$	0.79
300	17.1	$2.3 \times 10^7$	$2.4 \times 10^{-5}$	0.94	912.2	$3.1 \times 10^{-5}$	0.75
<b>Ringer pH = 8.91</b>							
24	17.6	$1.9 \times 10^6$	$6.3 \times 10^{-5}$	0.90	110.2	$7.5 \times 10^{-5}$	0.81
100	17.3	$4.1 \times 10^6$	$4.8 \times 10^{-5}$	0.91	415.6	$5.9 \times 10^{-5}$	0.77
300	16.9	$6.3 \times 10^6$	$4.1 \times 10^{-5}$	0.92	835.4	$1.3 \times 10^{-5}$	0.74
<b>Ringer-Brown pH = 7.4</b>							
24	17.9	$4.3 \times 10^6$	$3.9 \times 10^{-5}$	0.92	220.1	$5.9 \times 10^{-5}$	0.84
100	17.5	$9.3 \times 10^6$	$2.8 \times 10^{-5}$	0.95	543.2	$4.2 \times 10^{-5}$	0.80
300	17.2	$2.7 \times 10^7$	$2.1 \times 10^{-5}$	0.96	957.2	$2.9 \times 10^{-5}$	0.76

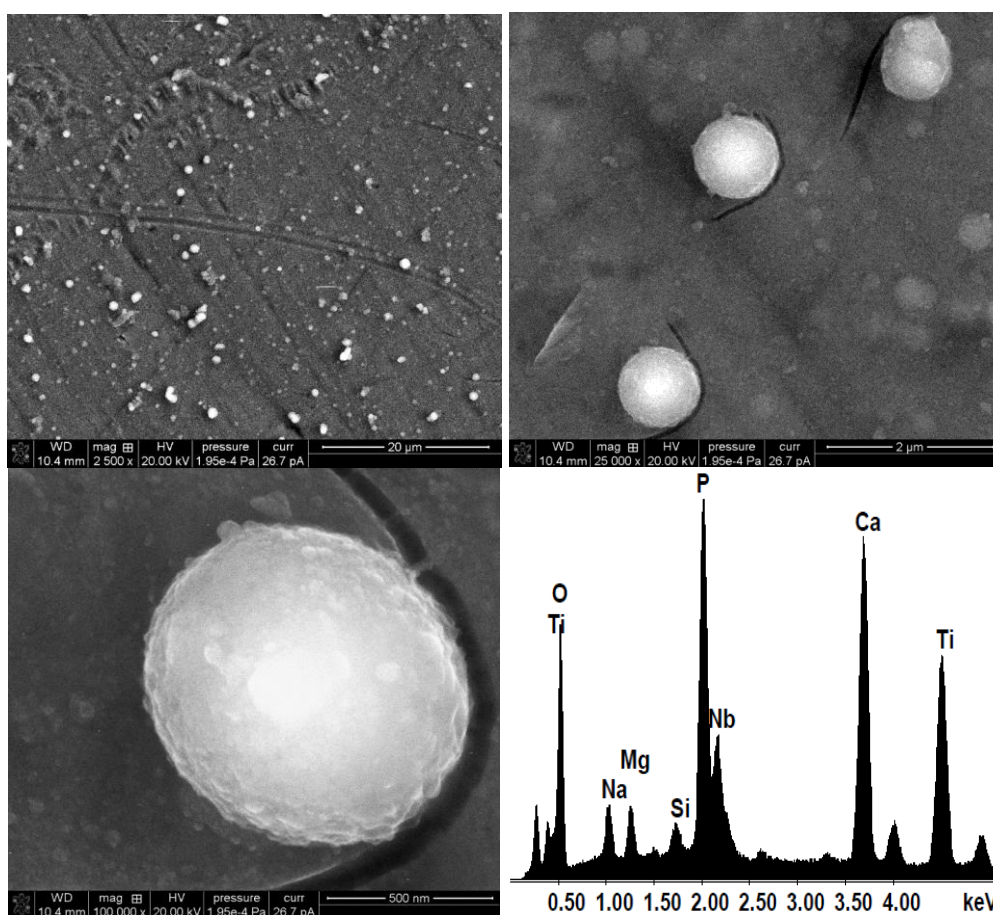


**Figure 7.** SEM micrographs (at different magnifications) and EDS spectra of galvanostatic oxidation Ti-20Nb-10Zr-5Ta alloy surface after 300 immersion hours in neutral Ringer solutions.

It results that the new layer deposited from the simulated physiological solutions contains calcium phosphates as was demonstrated by EDS analysis; these calcium phosphates are precursors of the hydroxyapatite, the main inorganic component of the human bone; therefore, the primary oxidation

layer favoured the deposition of these compounds which can stimulate the formation of the hydroxyapatite; thus, the alloy surface becomes bioactive.

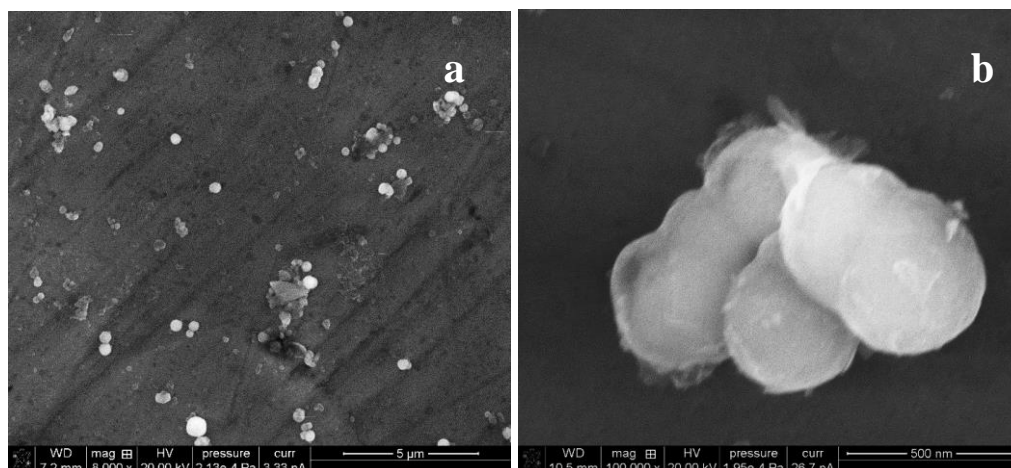


**Figure 8.** SEM micrographs of galvanostatic oxidation Ti-20Nb-10Zr-5Ta alloy surface after 300 immersion hours in: a) alkaline Ringer solution; b) neutral Ringer-Brown solution.

#### 4. CONCLUSIONS

By galvanostatic oxidation of Ti-20Nb-10Zr-5Ta alloy in 1M H<sub>3</sub>PO<sub>4</sub> solution, a thick porous layer was obtained. This layer is formed by amorphous TiO<sub>2</sub> and contains anatase inclusions. Cyclic potentiodynamic polarisation curves in simulated physiological solutions revealed that all main electrochemical parameters exhibited more favourable values for the galvanostatic oxidation alloy than those for the bare one, confirming a nobler behaviour of the coated alloy, due to the barrier properties of the oxidation layer. These parameters improved their values in time, showing that on the primary layer were deposited new layers from the simulated biofluids. For the galvanostatic oxidation alloy, the values of the polarisation resistances increased and corrosion and ion release rates decreased in time, indicating the thickening of the oxidation layer due to the depositions from the solutions. All impedance parameters increased with the soaking time, as result of the new protective layer deposited from the electrolyte. An electric equivalent circuit with two time constants was modelled: the first constant is for the barrier layer and the second constant characterise the porous layer deposited from solution. SEM micrographs and EDS elemental analysis showed that the coating deposited after 300 immersion hours in Ringer and Ringer-Brown solutions contained calcium phosphates, precursors of the hydroxyapatite, the main inorganic component of the human bone, namely, the alloy surface became bioactive.

#### ACKNOWLEDGMENTS

This work was supported by Romanian CNCSIS - UEFISCDI, project number PN II – IDEI code 248/2010. Also, support of the EU (ERDF) and Romanian Government infrastructure POS-CCE O 2.2.1 project INFRANANOCHEM - No. 19/2009 is gratefully acknowledged.

## References

1. M. P. Neupane, I. S. Park, S. J. Lee, K. A. Kim, M. H. Lee and T.S. Bae, *Int. J. Electrochem. Sci.*, 4 (2009) 197
2. N. F. Fahim, M. F. Morks and T. Sekino, *Electrochim. Acta*, 54 (2009) 3255
3. J. Jakubowicz, G. Adamek, M. U. Jurczyk and M. Jurczyk, *Mater. Charact.*, 70 (2012) 55
4. Y. Shibata, D. Suzuki, S. Omori, R. Tanaka, A. Murakami, Y. Kataoka, K. Baba and R. Kamijo, *Biomaterials*, 31 (2010) 8546
5. R. Roest, B. A. Latella, G. Heness and B. Ben-Nissan, *Surf. Coat. Technol.*, 205 (2011) 3520
6. H. H. Park, I. S. Park, K. S. Kim, W. Y. Jeon, B. K. Park, H. S. Kim, T. S. Bae and M. H. Lee, *Electrochim. Acta*, 55 (2010) 6109
7. R. Narayanan and S. K. Seshadri, *Corros. Sci.*, 49 (2007) 542
8. V. S. Saji and H. C. Choe, *Corros. Sci.*, 51 (2009) 1658
9. J. Zhao, X. Wang, X. Wang and J. Zhou, *Int. J. Electrochem. Sci.*, 7 (2012) 11035
10. E. Eisenbarth, D. Velten, M. Muller, R. Thull and J. Breme, *Biomaterials*, 25 (2004) 5705
11. P. Thompsen, C. Larsson, L.E. Ericson, L. Sennerby, J. Lausama and B. Kasemo, *J. Mater. Sci.: Mater. Med.*, 8 (1997) 653
12. M. Popa, E. Vasilescu, P. Drob, D. Raducanu, J. M. Calderon Moreno, S. Ivanescu, C. Vasilescu and S. I. Drob, *Met. Mater. Int.*, 18 (2012) 639
13. M. V. Popa, I. Demetrescu, E. Vasilescu, P. Drob, A. Santana Lopez, J. Mirza Rosca, C. Vasilescu and D. Ionita, *Electrochim. Acta*, 49 (2004) 2113
14. C. Vasilescu, P. Drob, E. Vasilescu, I. Demetrescu, D. Ionita, M. Prodana and S. I. Drob, *Corros. Sci.*, 53 (2011) 992
15. E. Vasilescu, P. Drob, D. Raducanu, I. Cinca, D. Mareci, J.M. Calderon Moreno, M. Popa, C. Vasilescu and J.C. Mirza Rosca, *Corros. Sci.*, 51 (2009) 2885
16. E. Vasilescu, P. Drob, D. Raducanu, V. D. Cojocaru, I. Cinca, D. Iordachescu, R. Ion, M. Popa and C. Vasilescu, *J. Mater. Sci.: Mater. Med.*, 21 (2010) 1959
17. R. M. A. Shahba, W. A. Ghannem and A. El-Sayed El-Shenawy, *Int. J. Electrochem. Sci.*, 6 (2011) 5499
18. V. Raman, S. Tamilselvi and N. Rajendran, *Electrochim. Acta*, 52 (2007) 7418
19. L. T. Duarte, S. R. Biaggio, R. C. Rocha-Filho and N. Bocchi, *J. Mater. Sci.: Mater. Med.*, 22 (2011) 1663
20. J. Black, *Biological performance of materials: Fundamentals of biocompatibility*, M. Decker Inc. New York, 1992
21. D. J. Blackwood, A. W. C. Chua, K. H. W. Seah, R. Thampuran and S. H. Teoh, *Corros. Sci.*, 42 (2000) 481
22. P. Mondragon-Cortez and G. Vargas-Gutierrez, *Mater. Lett.*, 58 (2004) 133
23. A. K. Shukla and R. Balasubramaniam, *Corros. Sci.*, 48 (2006) 1696
24. A. W. E. Hodgson, Y. Mueller, D. Forster and S. Virtanen, *Electrochim. Acta*, 47 (2002) 1913
25. O. R. Camara, L. B. Avalle and F. Y. Oliva, *Electrochim. Acta*, 55 (2010) 4519
26. Q. Mohsen and S. A. Fadl-Allah, *Mater. Corros.*, 62 (2011) 310
27. C. X. Wang, M. Wang and X. Zhou, *Biomaterials*, 24 (2003) 3069
28. S. Tamilselvi and N. Rajendran, *Mater. Corros.*, 58 (2007) 285
29. J. Pan, D. Thierry and C. Leygraf, *Electrochim. Acta*, 41 (1996) 1143
30. A. M. Fekry and M. A. Ameer, *Int. J. Electrochem. Sci.*, 6 (2011) 1342-1354
31. C. Sola, A. Amorim, A. Espias, S. Capelo, J. Fernandes, L. Proenca, L. Sanchez and I. Fonseca, *Int. J. Electrochem. Sci.*, 8 (2013) 406